Comparative analysis of the efficacy and safety of antibody-drug conjugates, radionuclide-drug conjugates and their combination targeting claudin 18.2 in gastric cancer treatment

HUAN DU[1,2], XIAO-FEI HAO[1], BIN-WEI LIN[1-3], YU ZHANG[1-3], LUO RUI[4], JING WANG[5,6], MING-MING TANG[7], DE-CAI WANG[1-3], YI-HAN ZHU[1-3], JIE LI[1-3], TANG-ZHI DAI[1-3], YUCHUAN YANG[5,6], XIA YANG[5,6] and XIAOBO DU[1-3]

[1]Mianyang Central Hospital, School of Medicine, University of Electronic Science and Technology of China, Mianyang, Sichuan 621000, P.R. China; [2]National Health Commission Key Laboratory of Nuclear Technology Medical Transformation, Mianyang Central Hospital, School of Medicine, University of Electronic Science and Technology of China, Mianyang, Sichuan 621000, P.R. China; [3]Sichuan Clinical Research Center for Radiation and Therapy, Mianyang Central Hospital, Mianyang, Sichuan 621000, P.R. China; [4]Department of Nuclear Medicine, Central Hospital of Mianyang, Mianyang, Sichuan 621000, P.R. China; [5]Institute of Nuclear Physics and Chemistry, China Academy of Engineering Physics, Mianyang, Sichuan 621900, P.R. China; [6]Targeted Radiopharmaceuticals Creation Key Laboratory of Sichuan Province, Mianyang, Sichuan 621900, P.R. China; [7]Department of Clinical Medicine, Clinical Medical School, North Sichuan Medical College, Nanchong, Sichuan 637007, P.R. China

Received June 27, 2025; Accepted September 29, 2025

DOI: 10.3892/or.2025.9009

Abstract. Gastric cancer (GC) is one of the most common types of cancer worldwide, with limited therapeutic options available for patients with advanced-stage disease. Claudin 18.2 (CLDN18.2) has emerged as a popular target for the diagnosis and treatment of GC. Although antibody-drug conjugates (ADCs) and radionuclide-drug conjugates (RDCs) targeting CLDN18.2 have been assessed, to the best of our knowledge, no comparative studies have evaluated the efficacy and toxicity profiles of these two treatment modalities. The present study aimed to compare the antitumor efficacy and toxicity of ADCs and RDCs derived from the same anti-CLDN18.2 monoclonal antibody (mAb) targeting CLDN18.2-positive tumors. Modified DFO/DOTA-SYSA1801mAb, labeled with ^{89}Zr and ^{177}Lu, was used in cell-based assays, positron emission tomography and biodistribution studies to evaluate its targeting specificity. In an NUGC-4-CLDN18.2 xenograft tumor model, the antitumor efficacy and toxicity of the mAb (SYSA1801mAb), as well as the ADC (SYSA1801) and RDC ([^{177}Lu]Lu-DOTA-SYSA1801mAb), and their combinations in different sequences (ADC→RDC and RDC→ADC), were systematically assessed. [^{89}Zr]Zr-DFO-SYSA1801mAb demonstrated notable *in vitro* stability and effectively imaged tumors with high CLDN18.2 expression. [^{177}Lu]Lu-DOTA-SYSA1801mAb exhibited strong tumor-targeting ability, with significantly higher tumor uptake than other tissues. By day 145, the complete remission (CR) rate in the ADC group was 60%, with an overall survival (OS) rate of 60%. In the ADC→RDC group, the CR and OS rates were both 40%. The OS rates in the RDC, RDC→ADC, mAb and control groups were all 0%. The ADC group exhibited minimal changes in hematological parameters and hepatic/renal function, whereas the RDC and RDC→ADC groups showed more significant changes. These preclinical findings suggested that ADC monotherapy may demonstrate superior efficacy and safety profiles when compared with RDC monotherapy. Furthermore, sequential combination therapy that starts with ADC appears to be more favorable than approaches that start with RDC. Although ADC→RDC sequential therapy did not significantly outperform ADC monotherapy in this model, it may serve as an effective subsequent treatment strategy.

Correspondence to: Professor Xiaobo Du, Mianyang Central Hospital, School of Medicine, University of Electronic Science and Technology of China, 12 Changjiaxiang, Mianyang, Sichuan 621000, P.R. China
E-mail: duxiaobo2005@126.com

Professor Xia Yang, Institute of Nuclear Physics and Chemistry, China Academy of Engineering Physics, 64 Mianshan Road, Youxian, Mianyang, Sichuan 621900, P.R. China
E-mail: yangxia.youka@caep.cn

Abbreviations: CLDN18.2, claudin 18.2; ADC, antibody-drug conjugate; RDC, radionuclide-drug conjugate; ALB, albumin; ALT, alanine aminotransferase; AST, aspartate aminotransferase; BUN, blood urea nitrogen; CREA, creatinine; UA, uric acid; WBC, white blood cells; RBC, red blood cells; PLT, platelets; OS, overall survival; CR, complete remission

Key words: CLDN18.2, SYSA1801, ADC, 177Lu, gastric cancer

Introduction

In 2022, gastric cancer (GC) was reported to be the fifth most common cancer worldwide, with ~968,000 new cases diagnosed globally (1). Although various treatment modalities have been developed for GC and other cancer types, including surgery, chemotherapy, radiotherapy, immunotherapy and targeted therapy, therapeutic outcomes remain suboptimal, particularly in the advanced stages (2). Surgery is the primary treatment option for early-stage GC; however, its efficacy diminishes in locally advanced or metastatic disease (3). Chemotherapy is widely used in advanced settings; however, it is often associated with severe systemic toxicities that limit long-term application (4). Radiotherapy is primarily used for palliative symptom control or as an adjuvant treatment; however, it has limited effectiveness in improving overall survival (OS) in metastatic GC (5,6). Immunotherapy has shown promising efficacy in certain subgroups, such as in patients with high microsatellite instability or Epstein-Barr virus-positive GC; however, response rates remain low in unselected populations (7,8). Traditional Chinese medicine, including herbal formulations and acupuncture, has been integrated into supportive cancer care to alleviate treatment-related side effects and to improve quality of life, although robust evidence from large-scale randomized controlled trials supporting its direct antitumor efficacy is still lacking (9-13). Biomarker-driven targeted therapies are effective in patients with specific molecular alterations; however, they offer no benefit to most patients with GC lacking these targets (14). Consequently, despite the diversity of available treatments, the annual number of GC-related deaths remains as high as 660,000 globally (15), indicating the urgent need to develop more effective and better-tolerated therapeutic strategies for GC.

Claudin 18.2 (CLDN18.2) is highly and specifically expressed in GC (16,17), making it a primary target for precision therapy (18). Beyond its role as a surface biomarker, CLDN18.2 contributes to gastric oncogenesis through multifaceted mechanisms (19). In normal gastric mucosa, CLDN18.2 is exclusively localized to the tight junctions of polarized epithelial cells; however, in gastric cancer, neoplastic cells frequently lose their polarity, leading to the mislocalization of CLDN18.2, characterized by its diffuse presence over the entire cell membrane rather than being confined to the apical junction complex (17). Its aberrant expression and mislocalization in GC disrupt tight junction integrity and epithelial polarity, thereby enhancing tumor cell invasion and metastasis (20,21). Furthermore, CLDN18.2 is implicated in pro-tumorigenic signaling, potentially through interactions with integrins to activate FAK/SRC, PI3K/AKT and MAPK/ERK pathways, which promote cell proliferation, survival and migration (22). This protein also influences the tumor immune microenvironment (23,24); high CLDN18.2 expression is associated with altered immune cell infiltration (such as increased $CD68^+$ macrophage levels) and may contribute to an immunosuppressive context, potentially affecting responses to immunotherapy (25,26). These biological roles provide a strong rationale for targeting CLDN18.2, as its inhibition may not only deliver cytotoxic agents directly to tumor cells but also counteract its functional oncogenic drivers.

Based on existing data, the relationship between CLDN18.2 expression and OS in patients with GC or gastroesophageal junction cancer is complex and remains controversial. It has been indicated that a CLDN18.2-negative status may be associated with a longer OS (27,28), whereas other studies have reported that CLDN18.2 positivity is linked to improved OS (26,29). However, several studies have found no notable association between CLDN18.2 expression and OS or histopathological subtypes (30-32). A 2021 meta-analysis of six studies concluded that there was no significant difference in OS between CLDN18.2-positive and CLDN18.2-negative groups (33). Therefore, CLDN18.2 is generally not recommended as an independent prognostic biomarker for OS in patients with GC (20). Instead, CLDN18.2 has a more consistent, evidence-based role as a predictive biomarker, indicating the potential benefits of targeted therapy.

In recent years, studies on targeted therapies against CLDN18.2, including monoclonal antibodies (mAbs), bispecific antibodies, antibody-drug conjugates (ADCs) and radionuclide-drug conjugates (RDCs) (34-36), have advanced rapidly. Among these, zolbetuximab, a CLDN18.2 mAb, has demonstrated limited efficacy in clinical trials (37-39). However, ADCs and RDCs developed based on CLDN18.2 mAb, such as CLDN18.2-307-ADC (40) and [^{177}Lu]Lu-TST001, have shown marked antitumor effects and controllable safety profiles (41).

Both ADCs and RDCs achieve precise treatment through specifically targeting tumor cells (42,43). ADCs deliver cytotoxic drugs directly to tumor cells using mAbs to recognize tumor cell-surface antigens with high specificity, thereby minimizing toxicity to normal tissues (44). By contrast, RDCs utilize tumor-targeting molecules labeled with radioactive isotopes to provide precise radiation therapy, and demonstrate strong cytotoxic effects against local refractory lesions or metastatic sites (45). However, both classes of drugs face inherent challenges; ADCs may experience reduced efficacy owing to the development of resistance, whereas RDCs may cause radiation-related side effects (46).

Existing data have indicated that ADCs and RDCs demonstrate superior antitumor efficacy compared with CLDN18.2 mAbs, with controllable safety profiles (47). However, studies comparing the antitumor efficacy and safety of ADCs and RDCs, as well as those exploring their combination are lacking. To the best of our knowledge, the current study is the first to systematically compare the antitumor efficacy and safety of ADCs, RDCs and their sequential combination regimens. The findings of the present study may provide preclinical evidence to guide future clinical applications of ADCs and RDCs. Specifically, identifying the treatment modality or combination sequence that exhibits superior efficacy and safety will be invaluable for designing clinical trials and selecting therapeutic strategies for patients with CLDN18.2-positive tumors. This comparative strategy may also serve as a paradigm for evaluating novel targeted conjugates beyond CLDN18.2. Therefore, the present study aimed to utilize ADC (SYSA1801) and RDC ([^{177}Lu]Lu-DOTA-SYSA1801mAb) agents derived from the same CLDN18.2 mAb (SYSA1801mAb) and to compare their efficacy and safety in the treatment of CLDN18.2-positive GC. In addition, the potential of their combined treatment strategies was evaluated.

Materials and methods

Cell culture. The human GC cell line NUGC-4-CLDN18.2 was purchased from Chengdu Besidi Biotechnology Co., Ltd. This cell line was generated by the vendor through lentiviral transduction to stably express CLDN18.2, and its expression was confirmed by them. in addition, the cell line was authenticated by short tandem repeat (STR) profiling (Genetic Testing Biotechnology Co., Ltd.). The STR profile matched the reference profile for NUGC-4 (DSMZ database, https://www.dsmz.de) at all eight core loci and amelogenin. The NUGC-4-CLDN18.2 cells were cultured in Roswell Park Memorial Institute 1640 medium (Gibco; Thermo Fisher Scientific, Inc.) supplemented with 10% fetal bovine serum (FBS; Gibco; Thermo Fisher Scientific, Inc.), 1% penicillin-streptomycin and 0.5% puromycin. Cultures were maintained at 37˚C in a 5% CO_2 incubator.

Animal models. Female BALB/c-nu mice (n=48; age, 6-8 weeks; weight, 18-22 g) were purchased from SPF Biotechnology Co., Ltd. and housed under specific pathogen-free (SPF) conditions. The housing environment was maintained at a temperature of 22±2˚C, 50±10% humidity, under a 12/12-h light/dark cycle. Mice had *ad libitum* access to a standard SPF rodent diet and water. For the subcutaneous xenograft model, $1x10^7$ NUGC-4-CLDN18.2 cells in 100 μl PBS were injected into the right dorsal flank of each mouse (48,49). Tumor-bearing mice were then allocated to the following studies: 30 mice for the therapeutic efficacy experiment (6 groups; n=5), 15 mice for biodistribution studies (n=3 mice per time point across five time points) and 3 mice for positron emission tomography-computed tomography (PET/CT) imaging. The experiment was initiated when tumor volumes reached ~300 mm^3. Humane endpoint criteria were strictly followed, and mice were euthanized immediately if the tumor volume exceeded 2,000 mm^3 or if there was a 20% decrease in body weight relative to the baseline (day 0). All animal experiments were approved by the Animal Ethics Committee of Mianyang Central Hospital (ethical approval no. S20240210; Mianyang, China).

Source of SYSA1801mAb. SYSA1801mAb is a fully human mAb targeting CLDN18.2, which was developed by and sourced from CSPC Pharmaceutical Holdings Group Ltd. Detailed information regarding antibody production, plasmid structure and amino acid sequences remains confidential. SYSA1801mAb was used to generate both diagnostic and therapeutic radioconjugates. For PET imaging, the antibody was conjugated to DFO and labeled with ^{89}Zr to form [^{89}Zr]Zr-DFO-SYSA1801mAb. For biodistribution studies and therapeutic purposes, the antibody was conjugated to DOTA and labeled with ^{177}Lu to form the therapeutic radioconjugate [^{177}Lu]Lu-DOTA-SYSA1801mAb (referred to as RDC).

Flow cytometry of cell lines. First, $5x10^4$ cells/well were pre-seeded in a 96-well U-bottom cell culture plate, and were centrifuged at 200 x g for 5 min at 4˚C. The pellets were then resuspended and washed twice with ice cold fluorescence-activated cell sorting (FACS) buffer (95% PBS and 5% FBS). Subsequently, the cells were incubated in 50 μl anti-human CLDN18.2 mAb (SYSA1801mAb) for 60 min at 4˚C. The concentration of the antibody added to the first well was 15 μg/ml, followed by twelve serial two-fold dilutions. Then, the cells were incubated in the dark for 30 min at 4˚C with a R-phycoerythrin-conjugated goat anti-human IgG secondary antibody (1:1,000; cat. no. 12499882; eBioscience; Thermo Fisher Scientific, Inc.). After incubation, the cells were washed twice with FACS buffer, as aforementioned. The cells were resuspended in 200 μl FACS buffer for analysis in a FACSCalibur flow cytometer (Beckman Coulter, Inc.). Data for 3,000 cells were collected and analyzed using the BD FlowJo software (version v2.1.0; BD Biosciences).

Synthesis of SYSA1801mAb-DFO. SYSA1801mAb stock solution was added to an ultrafiltration tube [molecular weight cut-off (MWCO), 30 kDa; MilliporeSigma] and centrifuged at 14,000 x g for 10 min at 4˚C to remove the solvent from the stock solution. A suitable volume of buffer A solution (Na_2CO_3-$NaHCO_3$, pH 9.5, 0.15 M) was added, and the mixture was immediately centrifuged (14,000 x g for 10 min at 4˚C). This procedure was repeated three times. The purified antibody was then transferred to a 1.5-ml centrifuge tube, 10 times the molar mass ratio of p-NCS-Bz-DFO [20 nmol/μl, dissolved in dimethyl sulfoxide (DMSO)] was added, gently blown on and mixed well. The mixture was then incubated at a constant temperature of 37˚C on a shaker for 1 h at 70 rpm. Subsequently, the antibody was transferred to an ultrafiltration tube. Following the addition of buffer C solution (NaOAc-Ac, pH 5.5, 0.5 M), it was centrifuged at 14,000 x g for 10 min at 4˚C, a process that was repeated three times to remove the solvent.

Synthesis of SYSA1801mAb-DOTA. SYSA1801mAb was added to an ultrafiltration tube (MWCO, 30 kDa; Chelex 100 sodium form), and the solvent in the stock solution was removed by centrifugation at 14,000 x g for 10 min at 4˚C. A suitable volume of buffer A solution (Na_2CO_3-$NaHCO_3$, pH 9.5, 0.15 M) was added, and the mixture was immediately centrifuged (14,000 x g for 10 min at 4˚C). This procedure was repeated three times. The purified antibody was then transferred to a 1.5-ml centrifuge tube and 10 times the molar mass ratio of p-NCS-Bz-DOTA (20 nmol/μl, dissolved in DMSO) was added. The mixture was incubated at a constant temperature of 37˚C on a shaker for 1 h at 70 rpm. Subsequently, the antibody was transferred to an ultrafiltration tube. Following the addition of buffer C solution (NaOAc-Ac, pH 5.5, 0.5 M), it was centrifuged at 14,000 x g for 10 min at 4˚C, a procedure that was repeated three times to remove the solvent.

Synthesis of [^{89}Zr]Zr-DFO-SYSA1801mAb. High-purity yttrium foil (purity >99.99%, specification: 11x16x0.65 mm; Suzhou Changyou Gas Co., Ltd.) was procured as the target material and then irradiated with a cyclotron to induce nuclear reactions. After irradiation, the target material was subjected to acid dissolution and purification to obtain ^{89}Zr with acceptable radioactivity and chemical purity in the form of [^{89}Zr]Zr-oxalate. [^{89}Zr]Zr-oxalate was added to the centrifuge tube, and the pH was adjusted to ~7.0 with solution B (0.5 M Na_2CO_3) and left at room temperature for 3 min. SYSA1801mAb-DFO was then added to the solution at a 1:2 labeling ratio, and

2-[4-(2-hydroxyethyl) piperazin-1-yl] ethanesulfonic acid solution was added to the centrifuge tube according to solution B and total volume of ^{89}Zr. The mixture was reacted in a metal bath at 37˚C for 90 min, shaking the solution by hand every 10 min. At the end of the reaction, the labeling rate of the samples was determined using thin-layer chromatography (TLC) (50).

Synthesis of [^{177}Lu]Lu-DOTA-SYSA1801mAb. To synthesize [^{177}Lu]Lu-DOTA-SYSA1801mAb, SYSA1801mAb-DOTA and $^{177}LuCl_3$ (sourced from the Institute of Nuclear Physics and Chemistry, China Academy of Engineering Physics, Mianyang, China) were combined at a 1:2 ratio and incubated the mixture for 1 h at 42˚C in a metal bath. After the reaction, the labeling rate of the samples was determined using TLC. Microfiber cellophane (cat. no. SG10001; iTLC-SG-Glass microfiber chromatography paper impregnated with silica gel; Agilent Technologies, Inc.) was cut into long strips of paper (10 cm long and 1.5 cm wide), and a marked line was drawn 1.5 cm from the bottom as a scale for spiking. Subsequently, 2 μl of the radioactive sample was pipetted to the marked line of the microfiber glassine strip, which was placed into a sodium citrate unfolding system after spotting (sodium citrate-citric acid, 0.5 M, pH 5.5). The reaction mixture was analyzed by high-performance liquid chromatography (HPLC) using an Agilent 1260 Infinity II system (Agilent Technologies, Inc.) to determine the radiochemical purity. The separation was performed on an Agilent XDB-C18 reversed-phase analytical column (4.6x250 mm, 5 μm; Agilent Technologies, Inc.) maintained at 25˚C. A sample volume of 30 μl was injected. The mobile phase consisted of water with 0.1% trifluoroacetic acid (TFA) and acetonitrile with 0.1% TFA. The purification method was as follows: The column was initially conditioned and washed with 0.1% TFA in water, then eluted with a linear gradient of 13 to 33% acetonitrile (with 0.1% TFA) in water over 20 min at a flow rate of 1 ml/min. Radio-HPLC detection was performed using a γ-radiation detector for ^{177}Lu, and ultraviolet-HPLC detection was carried out at 254 nm absorption.

In vitro stability. To determine *in vitro* stability, 10 μl [^{177}Lu]Lu-DOTA-SYSA1801mAb was added separately to 15 μl saline, and to 15 μl 1640 medium containing 10% FBS. The mixture was left at room temperature, and the labeling rate was determined by TLC at 4, 24, 48, 96 and 168 h for the two groups.

Binding assays. [^{177}Lu]Lu-DOTA-SYSA1801mAb was prepared as aforementioned and the radiochemical purity of [^{177}Lu]Lu-DOTA-SYSA1801mAb was >99%. For the subsequent experiment, NUGC-4-CLDN18.2 cells ($1x10^5$ cells/well) were placed into a 100-μl centrifuge tube. The total binding of [^{177}Lu]Lu-DOTA-SYSA1801mAb was determined by adding it to cell suspensions at concentrations of 0.025-10.000 nM. Non-specific binding was determined by adding 50X half maximal effective concentration (EC_{50}) cold SYSA1801mAb to NUGC-4-CLDN18.2 cell mixtures at one concentration. The cells were incubated with 5 μCi [^{177}Lu]Lu-DOTA-SYSA1801mAb for 1 h at room temperature and washed three times with FACS buffer (95% PBS and 5% FBS). Bound and unbound radioactive fractions were collected and measured using a gamma counter (GC-1500; ANHUI USTC Zonkia Scientific Instruments Co., Ltd.). Saturation binding capacity (B_{max}) and EC_{50} values were calculated using PRISM v9.0 (Dotmatics).

PET/CT imaging. Tumor-bearing mice were sedated with isoflurane (2.0-2.5% in 2 l/min air) for intravenous injection of 4 MBq (104 μg) [^{89}Zr]Zr-DFO-SYSA1801mAb for PET/CT imaging. During the uptake periods (4, 24, 48, 96, 144 and 192 h post-injection), the mice were housed individually in a temperature-controlled room with free access to food and water, minimizing stress-related metabolic changes. Before PET/CT, the mice were re-anesthetized, placed on a heated imaging bed (37±0.5˚C), and monitored to maintain stable body temperature and respiration (respiratory rate: 60-80 breaths/min). Imaging was performed using Super Nova micro-PET/CT [PINGSENG Healthcare (Kunshan) Inc]. Spherical volumes of interest were delineated to encompass the tumor, major organs (the liver, spleen, kidney and heart), and background region (the thigh skeletal muscles). Decay-corrected injected activity, measured via pre- and post-injection weighing, and mouse body weight, recorded before the imaging, were used to calculate the percentage of injected dose per gram of tissue (%ID/g). This methodology was used to evaluate the target specificity of [^{89}Zr]Zr-DFO-SYSA1801mAb.

Biodistribution. Each tumor-bearing mouse was injected with 0.8 MBq (10 μg) [^{177}Lu]Lu-DOTA-SYSA1801mAb via the tail vein. As aforementioned, the mice were euthanized at selected time points (4, 24, 48, 96 and 144 h post-injection), with three mice per time point. Subsequently, major tissues and organs, including the heart, liver, spleen, lungs, kidneys, skeletal muscle (thigh muscle), femur (bone), whole blood, stomach, pancreas and intestines, were collected. All of the samples were blotted dry with a filter paper and weighed using an electronic balance.

The radioactivity of each sample was measured using an automated gamma counter (GC-1500; ANHUI USTC Zonkia Scientific Instruments Co., Ltd.) with a counting time of 10 sec. Background radioactivity was subtracted to correct the raw counts. The total injected radioactivity was determined by measuring the radioactivity of the injection syringe before and after administration (to account for residual radioactivity in the syringe). Tissue uptake was expressed as the %ID/g, calculated using the following formula: %ID/g=(corrected tissue radioactivity count/total injected radioactivity count) x (1/tissue wet weight) x100. Mouse biodistribution data (%ID/g) at multiple time points were converted to human organ %ID using the %kg/g scaling approach. For each organ, the scaled human %ID(t) was fitted with a bi-exponential model; the area under the fitted curve was integrated to infinity to derive the cumulated activity, which was then normalized by the administered activity (A_0) to yield the time-integrated activity coefficient: $\tau=(1/A_0)\int_0^{\wedge}\infty$ A_org(t) dt, reported in MBq·h/MBq.

ADC drug details. SYSA1801 (also known as EO3021; sourced from CSPC Pharmaceutical Holdings Group Ltd.) is an ADC drug that targets CLDN18.2. It consists of an mAb (SYSA1801mAb) that targets CLDN18.2 and monomethyl

auristatin E (MMAE), conjugated via a cleavable linker with a drug-to-antibody ratio (DAR) of 2. Detailed synthesis information is confidential. SYSA1801 is currently undergoing phase I clinical trials for the treatment of advanced solid tumors, demonstrating promising antitumor efficacy and manageable safety (NCT05009966).

Therapeutic dosing rationale and schedule

Dose selection. In BALB/c nude tumor-bearing mouse models, prior studies established 11.1 MBq as an appropriate dose for ^{177}Lu-labeled full-length mAb for therapeutic use (51,52). At this dose, the RDC demonstrated favorable tolerability, manageable toxicity and effective tumor growth suppression. Therefore, 11.1 MBq was selected as the single administration dose of RDC in the present study.

Antibody mass equivalence. To isolate payload effects, an identical mAb (SYSA1801mAb; 50 nmol/kg) was administered to RDC, ADC and mAb groups. This enabled a direct comparison of ^{177}Lu with cytotoxic drug efficacy under equivalent target engagement. For RDC preparation, a 1:2 antibody-to-^{177}Lu mass ratio was utilized, where 11.1 MBq RDC contained 150 μg antibody. To maintain antibody dose equivalence, both the ADC and mAb groups contained 150 μg per administration. The dosing for each group was as follows: [^{177}Lu]Lu-DOTA-SYSA1801mAb (11.1 MBq, 50 nmol/kg SYSA1801mAb), SYSA1801 (50 nmol/kg) and SYSA1801mAb (50 nmol/kg).

Grouping and intervention of tumor-bearing mice. Tumor-bearing mice were randomized into six groups (n=5/group), with interventions administered on days 0 and 14 as follows: The RDC group, 11.1 MBq (50 nmol/kg) [^{177}Lu]Lu-DOTA-SYSA1801mAb on days 0 and 14; the ADC group, 50 nmol/kg SYSA1801 on days 0 and 14; the ADC→RDC group, 50 nmol/kg SYSA1801 on day 0 and 11.1 MBq (50 nmol/kg) [^{177}Lu]Lu-DOTA-SYSA1801mAb on day 14; the RDC→ADC group, 11.1 MBq (50 nmol/kg) [^{177}Lu]Lu-DOTA-SYSA1801mAb on day 0 and 50 nmol/kg SYSA1801 on day 14; the mAb group, 50 nmol/kg SYSA1801mAb on days 0 and 14; the normal saline (NS) group, NS on days 0 and 14. Tumor-bearing mice were administered injections though the tail vein, with a dose volume of 200 μl/mouse. A schematic diagram of grouping and intervention for the tumor-bearing mice is shown in Fig. 1A.

Monitoring and subsequent testing. Tumor size and body weight of the mice were monitored starting from day 0 (first injection day). Tumor size was measured using a digital caliper, with the volume calculated as (length x width^2)/2 (length, longest diameter of the tumor; width, shortest diameter perpendicular to the length), and body weight was measured using an electronic balance. Both parameters were assessed on Tuesday and Friday after the first injection. The tumor growth inhibition rate (TGI%) was calculated as follows: TGI%=[1-(ΔT/ΔC)] x100, where ΔT is the change in mean tumor volume of the treatment group from baseline, and ΔC is the change in mean tumor volume of the control group from baseline.

The study endpoints were set as follows: i) Tumor volume reaching 2,000 mm^3 (triggering euthanasia); or ii) a 20% decrease in body weight relative to the baseline weight on day 0. Mice that did not meet these criteria were considered survivors for the purpose of the study. At these endpoints, the mice were anesthetized via inhalation of 5% isoflurane, and 500-800 μl blood was collected from the orbital venous plexus. Mice that reached predefined humane endpoints underwent blood collection from the orbital venous plexus and subsequent immediate euthanasia.

Animals were first anesthetized via inhalation of 5% isoflurane in an induction chamber. Upon loss of consciousness, the mice were transferred to a euthanasia chamber and exposed to 100% CO_2 at a flow rate displacing 40% of the chamber volume/min until respiratory arrest occurred. Death was subsequently confirmed by cervical dislocation. A portion of the blood sample was immediately used for routine hematological tests using an automated hematology analyzer (Mira BF; Shanghai RuiYu Biotech Co., Ltd.), and the remaining blood samples were centrifuged at 3,000 x g for 10 min at 4˚C to separate the serum, which was used for subsequent hepatorenal function tests using an automated biochemistry analyzer (BS-360S; Shenzhen Mindray Bio-Medical Electronics Co., Ltd.). Subsequently, major organs (the heart, liver, spleen, lung and kidney) were harvested, fixed in 4% paraformaldehyde for 24 h at room temperature, embedded in paraffin, and sectioned into 5-μm slices. The slices were stained with hematoxylin for 8 min and eosin for 3 min at room temperature, and observed under a light microscope (CX-31; Olympus Corporation) to evaluate histopathological changes (such as inflammatory cell infiltration, tissue necrosis and cellular degeneration), and to assess drug-induced hematological and organ toxicity.

Statistical analysis. Statistical analyses were performed using IBM SPSS Statistics for Windows (version 22.0; IBM Corp). For comparisons involving >2 groups, one-way analysis of variance was conducted, followed by Tukey's post hoc test for multiple comparisons where appropriate. $P<0.05$ was considered to indicate a statistically significant difference. Survival analysis was performed using Kaplan-Meier curves and differences between groups were assessed using the log-rank (Mantel-Cox) test. For the pre-specified pairwise comparisons among the four key treatment groups (RDC, ADC, ADC→RDC, RDC→ADC), a Bonferroni correction for multiple testing was applied. A total of six comparisons were conducted, resulting in a corrected significance threshold of $\alpha=0.0083$. Statistical significance for these pairwise comparisons was declared only when $P<0.0083$.

Results

Cell transfection and animal models. Flow cytometry confirmed a stable high expression of CLDN18.2 in the NUGC-4-CLDN18.2 cells (Fig. 1B). Finally, a subcutaneous positive GC xenograft model was established using NUGC-4-CLDN18.2 cells for subsequent animal experiments. When the NUGC-4-CLDN18.2 xenografts had grown to a volume of 732.75±197.96 mm^3, the therapeutic experiment was initiated.

Binding and stability. The integrity and radiochemical purity of [^{177}Lu]Lu-DOTA-SYSA1801mAb were determined to be >99% by HPLC using an Agilent 1260 Infinity II HPLC system (Fig. 1C). Subsequent incubation in NS and 1640

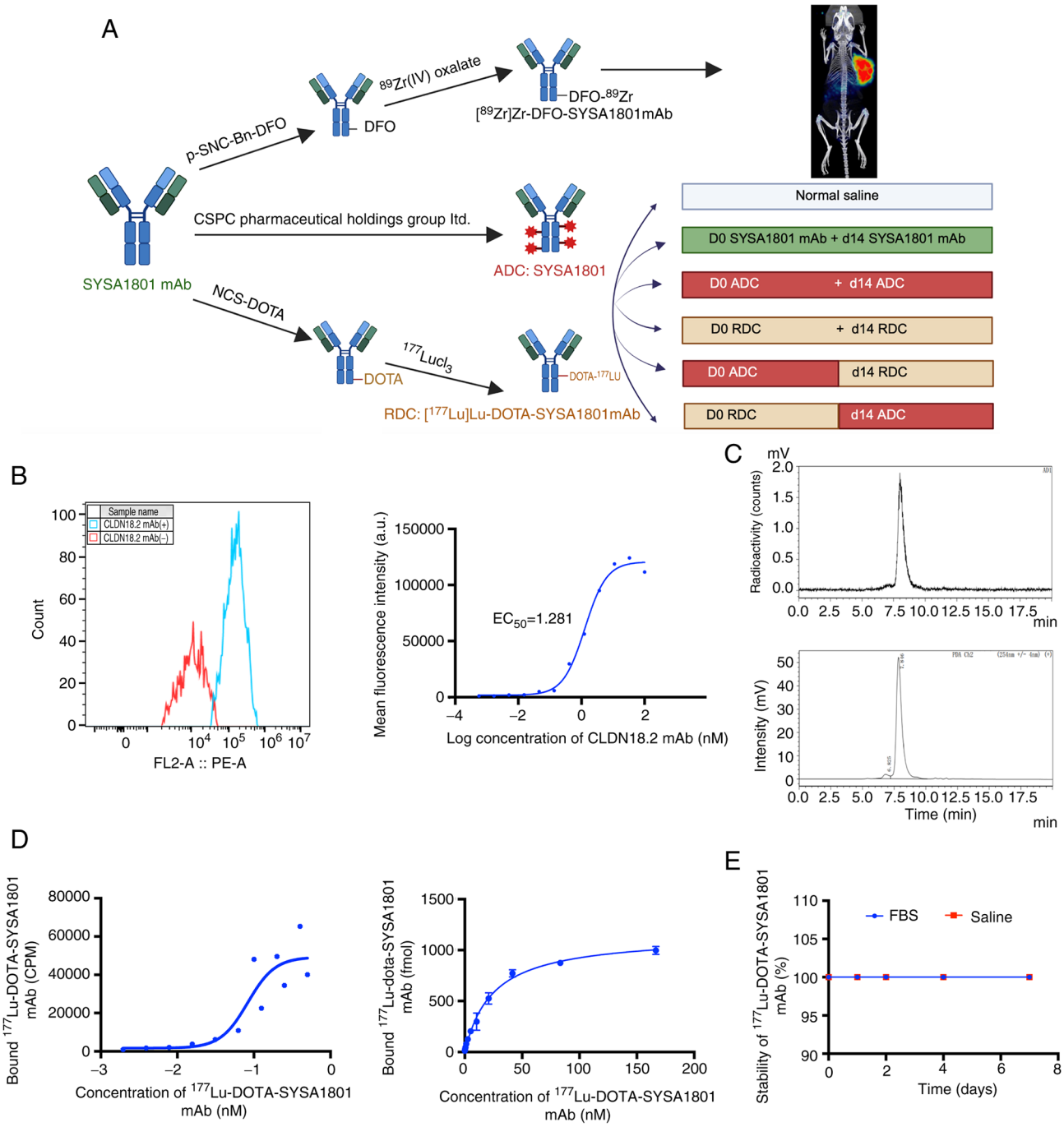

Figure 1. (A) Flow chart of the experimental design. Created with BioRender.com. (B) Flow cytometry was used to detect CLDN18.2 expression in NUGC-4-CLDN18.2 cells. Blue line: Anti-SYSA1801mAb (PE); red line: isotype control (PE). (C) Radiochemical purity of [^{177}Lu]Lu-DOTA-SYSA1801mAb determined by HPLC was >99%. Upper panel: Radio-HPLC (^{177}Lu γ-radiation detection); lower panel: Ultraviolet-HPLC (254 nm absorption detection). (D) Specific binding of [^{177}Lu]Lu-DOTA-SYSA1801mAb in NUGC-4-CLDN18.2 cells. Left panel: Saturation binding curve plotted on a logarithmic concentration scale for calculation of the equilibrium dissociation constant (Kd). Right panel: Saturation binding curve plotted on a linear concentration scale for determination of the maximum binding capacity (Bmax). (E) Stability of [^{177}Lu]Lu-DOTA-SYSA1801mAb detected by thin-layer chromatography in normal saline and 1640 (10% FBS). ADC, antibody-drug conjugate; CLDN18.2, claudin 18.2; EC_{50}, half maximal effective concentration; FBS, fetal bovine serum; HPLC, high-performance liquid chromatography; mAb, monoclonal antibody; RDC, radionuclide-drug conjugate.

medium (containing 10% FBS) for up to 7 days showed no degradation of [^{177}Lu]Lu-DOTA-SYSA1801mAb, as confirmed by radiolabeled TLC (Fig. 1E). Radioligand-binding assays were conducted using NUGC-4-CLDN18.2 cells. The B_{max} of [^{177}Lu]Lu-DOTA-SYSA1801mAb to NUGC-4-CLDN18.2 cells (1x0^5 cells) was 1,149±48.16 nmol, and the equilibrium dissociation constant was 24.36±3.5 nmol/l (Fig. 1D).

PET/CT imaging of [^{89}Zr]Zr-DFO-SYSA1801mAb. PET/CT imaging revealed that 4 h post-injection, [^{89}Zr]Zr-DFO-SYSA1801mAb accumulated in the tumor, with a clear tumor outline visible at 24 h post-injection (Fig. 2A). Over time, radioactive uptake in the tumor gradually increased. The maximum uptake of [^{89}Zr]Zr-DFO-SYSA1801mAb at the tumor site was observed at 48 h, with an uptake of ~4.94±1.06%ID/g

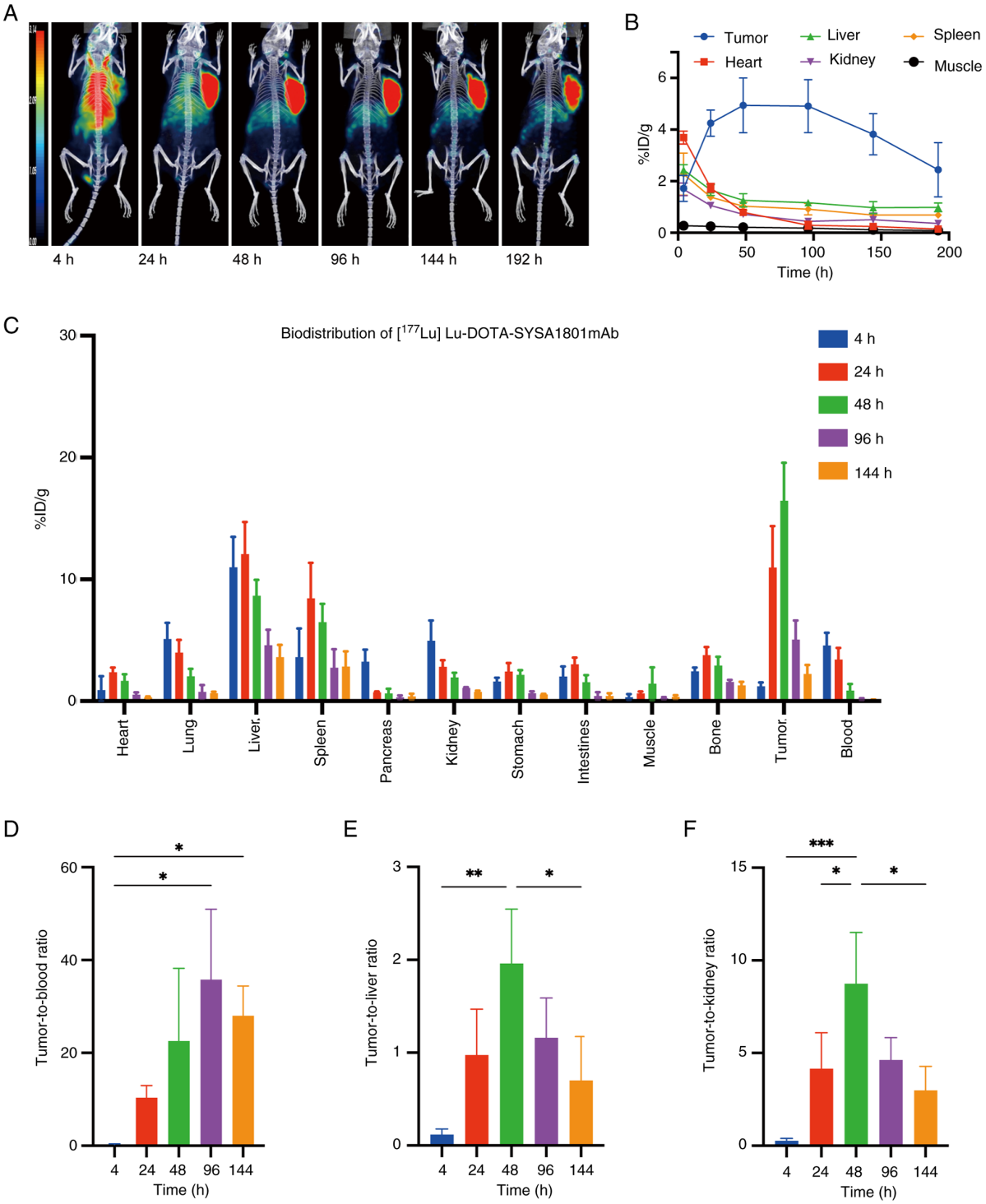

Figure 2. (A) Positron emission tomography-computed tomography images showing tumor-specific accumulation of [^{89}Zr]Zr-DFO-SYSA1801mAb in tumor-bearing mice over time, in contrast to that in other non-target tissues. (B) Quantitative region of interest analysis of the tumor, heart, liver, spleen, kidney, and muscle in tumor-bearing mice at 4, 24, 48, 96, 144 and 192 h after injection of [^{89}Zr]Zr-DFO-SYSA1801mAb. (C) Biodistribution results at 4, 24, 48, 96 and 144 h after injection of [^{177}Lu]Lu-DOTA-SYSA1801mAb. (D) Tumor-to-blood, (E) tumor-to-liver and (F) tumor-to-kidney ratios at 4, 24, 48, 96 and 144 h after injection of [^{177}Lu]Lu-DOTA-SYSA1801mAb. Data are presented as the mean ± SD. Statistical differences across the different time points for each ratio were determined by one-way analysis of variance followed by Tukey's post hoc test for multiple comparisons. *P<0.05, **P<0.01, ***P<0.001. %DI/g, percentage of injected dose per gram of tissue; mAb, monoclonal antibody.

(n=3) (Fig. 2B). Region of interest was further defined and radioactive uptake in the tumor, heart (blood), liver, spleen, muscle and kidneys was assessed. Radioactive uptake in non-target organs, such as the heart (blood), liver and kidneys, gradually decreased over time.

Biodistribution of [^{177}Lu]Lu-DOTA-SYSA1801mAb. Biodistribution results indicated that [^{177}Lu] Lu-DOTA-SYSA1801mAb effectively targeted tumors in the NUGC-4-CLDN18.2 model. Over time, tumor uptake increased, reaching a peak at 48 h (16.44±3.13%ID/g) (Fig. 2C).

Table I. Estimates of time-integrated activity coefficients for human organs from mouse biodistribution data.

Source organ	Kinetics value, MBq-h/MBq
Adrenal glands	0
Brain	0
Esophagus	0
Eyes	0
Gallbladder contents	0
Left colon	0
Small intestine	0.777
Stomach contents	0.268
Right colon	0
Rectum	0
Heart contents	$1.07x10^{1}$
Heart wall	0.566
Kidneys	0.246
Liver	$1.02x10^{1}$
Lungs	1.32
Pancreas	0.059
Prostate	0
Salivary glands	0
Red bone marrow	0
Cortical bone	$1.70x10^{1}$
Trabecular bone	0
Spleen	0.31
Testes	0
Thymus	0
Thyroid	0
Urinary bladder contents	0
Total body	0

Liver uptake peaked at 24 h (12.06±2.63%ID/g) and kidney uptake peaked at 4 h (4.96±1.66%ID/g). As time progressed, uptake in the liver and kidneys gradually decreased. Following blood circulation, [^{177}Lu]Lu-DOTA-SYSA1801mAb was rapidly cleared from the bloodstream. The concentration of radioactivity in the blood decreased by over 80% during the period from 4 and 48 h post-injection. Between 4 and 96 h post-injection, the tumor-to-blood ratio gradually increased, reaching a maximum ratio of 31.62±17.13 (Fig. 2D). Tumor-to-liver and tumor-to-kidney ratios exhibited fluctuating trends, with the highest values observed at 48 h (Fig. 2E and F). Dosimetry results are presented in Table I.

Effect of treatment. In the NUGC-4-CLDN18.2 model, the NS and mAb groups reached humane endpoints by day 14 post-treatment. The average tumor volume in the mAb group was 1,906.58±71.11 mm^3 (TGI%=4.57%), while in the NS group, it was 1,997.88±71.11 mm^3, with no significant difference between the two groups (Figs. 3A and S1). A total of 14 days after the first administration, in the RDC monotherapy group, the average tumor volume was 686.86±153.12 mm^3 (TGI%=105.32%), in the ADC group, it was 222.49±236.45 mm^3 (TGI%=139.80%), in the RDC→ADC group, it was 713.65±271.28 mm^3 (TGI%=100.60%), and in the ADC→RDC group, it was 278.79±381.72 mm^3 (TGI%=137.93%). Significant differences in tumor volume were observed between some treatment groups, and the detailed pairwise comparisons are presented in Table SI. On day 46 post-treatment, the average tumor volume in the RDC group was 871.63±503.97 mm^3, in the ADC group, it was 303.05±439.34 mm^3, in the RDC→ADC group, it was 941.74±803.32 mm^3, and in the ADC→RDC group, it was 248.31±474.01 mm^3. Significant differences in tumor volume were observed between the following pairs: RDC and ADC, RDC and ADC→RDC, ADC and RDC→ADC, and RDC→ADC and ADC→RDC. On day 14 post-treatment, the mice in the NS and mAb groups showed a gradual increase in body weight, whereas the mice in the other treatment groups experienced an initial weight decrease followed by a slow increase (Fig. 3B). Significant differences in weight were observed between some of the groups. Specifically, the ADC→RDC group showed a statistically significant difference compared with the ADC group, and the RDC group also differed significantly from the ADC group.

On day 46 post-treatment, the body weight of the mice in the RDC, ADC, ADC→RDC and RDC→ADC groups showed fluctuating increments, with no significant difference in body weight among the treatment groups (Table SII). On day 145 post-treatment, complete remission (CR) rate in the ADC group was 60%, with the OS rate also at 60%. In the ADC→RDC group, the CR rate was 40% and the OS rate was 40%, whereas the OS rate in the other groups was 0%. Statistically significant differences in OS rates were observed between the ADC and RDC groups, as well as between the ADC and RDC→ADC groups (Fig. 3C and D).

Toxicity of treatment. To comprehensively evaluate the potential adverse effects of these treatments, hematological, biochemical and histopathological analyses were conducted. Hematological analysis revealed elevated white blood cell counts in all treatment groups relative to the NS control group (Fig. 4A), with detailed results of pairwise comparisons between the groups provided in Table SIII. This elevation might suggest an inflammatory response or stress induced by treatment, which warrants further exploration of the impact on the immune system. Red blood cell counts showed minimal differences across groups, with a significant difference observed only between the ADC and mAb groups, and between the mAb and ADC→RDC sequential therapy groups. No significant differences were found in platelet counts among the groups. Levels of hepatocellular injury markers, alanine and aspartate aminotransferases exhibited only minor fluctuations across the treatment groups, with no significant differences observed (Fig. 4C). However, a significant decrease in albumin levels was noted in all the treatment groups, except the mAb group, compared with those in the NS group ($P<0.05$), suggesting a potential impairment of hepatic synthetic function, which is a known side effect of certain chemotherapeutic and targeted agents (51). More pronounced toxicological profiles were observed in the kidneys. Compared with those in the NS group, blood urea nitrogen (BUN), creatinine (Cr) and uric acid levels were elevated to varying degrees

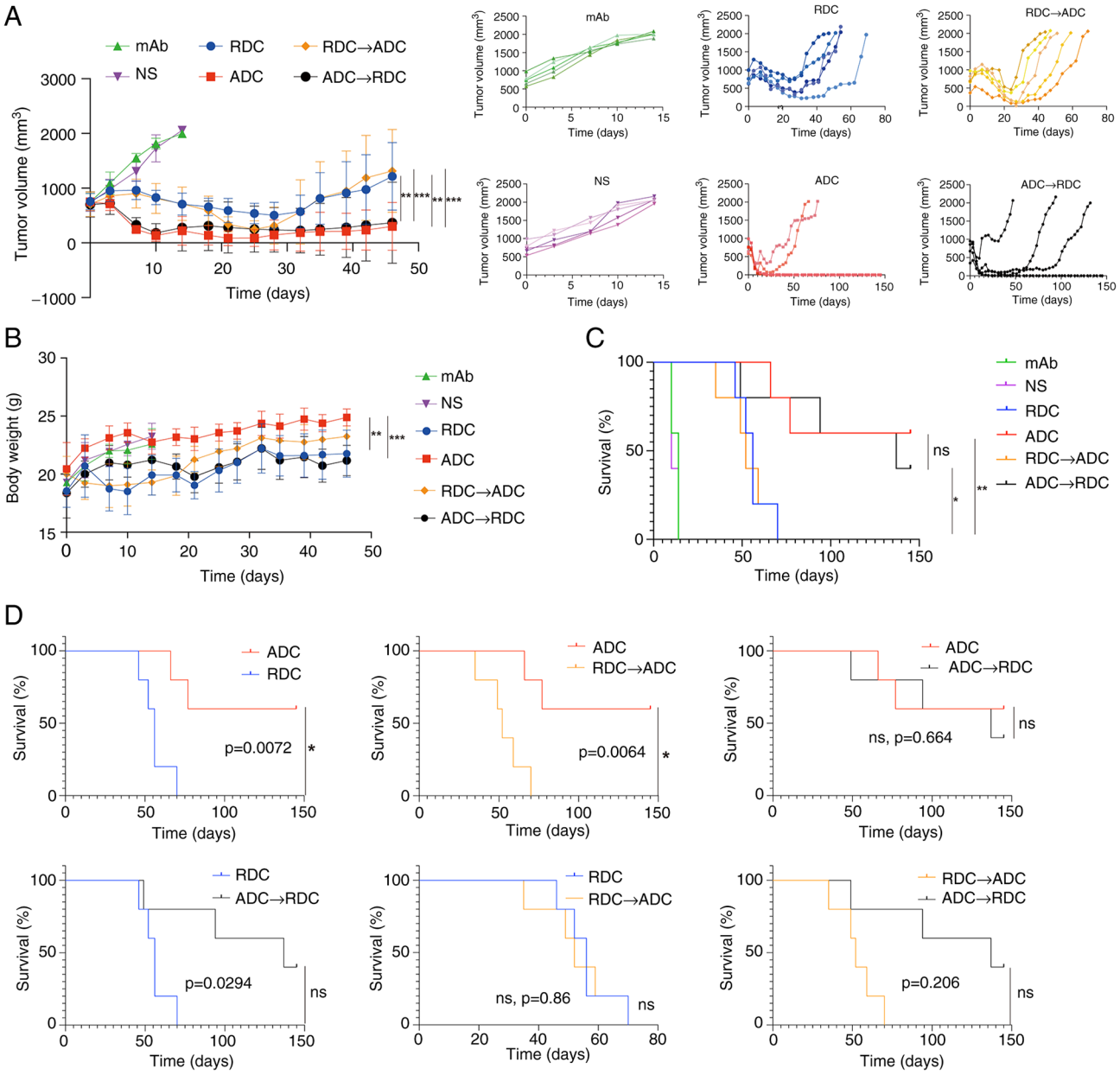

Figure 3. (A) Tumor growth curve of NUGC-4-claudin 18.2 model in each treatment group. (B) Body weight change curve for each treatment group. Statistical differences across the groups were determined by one-way analysis of variance followed by Tukey's post hoc test for multiple comparisons. *P<0.05, **P<0.01, ***P<0.001. (C) Kaplan-Meier survival curves comparing the survival probability of different treatment groups over time (n=5 mice/group). The log-rank (Mantel-Cox) test was used to determine statistical significance between groups. ***P<0.001. (D) Pairwise comparisons of survival among key treatment groups. The P-values result from post-hoc log-rank tests comparing the indicated groups, with a Bonferroni correction applied for six pre-specified comparisons (significance threshold: P<0.0083). *P<0.0083; ns, not significant. ADC, antibody-drug conjugate; mAb, monoclonal antibody; NS, normal saline; RDC, radionuclide-drug conjugate.

in the treatment groups, with relatively greater changes in the combination treatment and RDC groups (Fig. 4C; Table SIII). This consistent pattern suggests a potential impairment of the glomerular filtration rate and renal function.

Histopathological examination provided evidence for the biochemical findings (Fig. 4D). Although the architecture of the heart, lungs and liver remained intact across all the groups, notable changes were observed in the kidneys and spleen. Specifically, the mice treated with RDC and combination therapy exhibited partial damage and deformation of glomeruli and renal tubules, consistent with renal function deterioration, as indicated by elevated BUN and Cr levels. Disruption of the splenic follicular structure was also observed in these groups. These changes were markedly milder in the ADC and mAb monotherapy groups compared with those in the RDC and combination therapy groups. Cardiac, pulmonary and hepatic tissues remained largely intact across all the groups, with no signs of notable drug-induced injury.

Overall, the toxicity profile indicated that RDC and the combination therapy were associated with controllable but notable nephrotoxicity and potential effects on hepatic synthetic function. The absence of marked histopathological damage in the heart and lungs suggests favorable cardiotoxicity and pulmonary toxicity safety profiles.

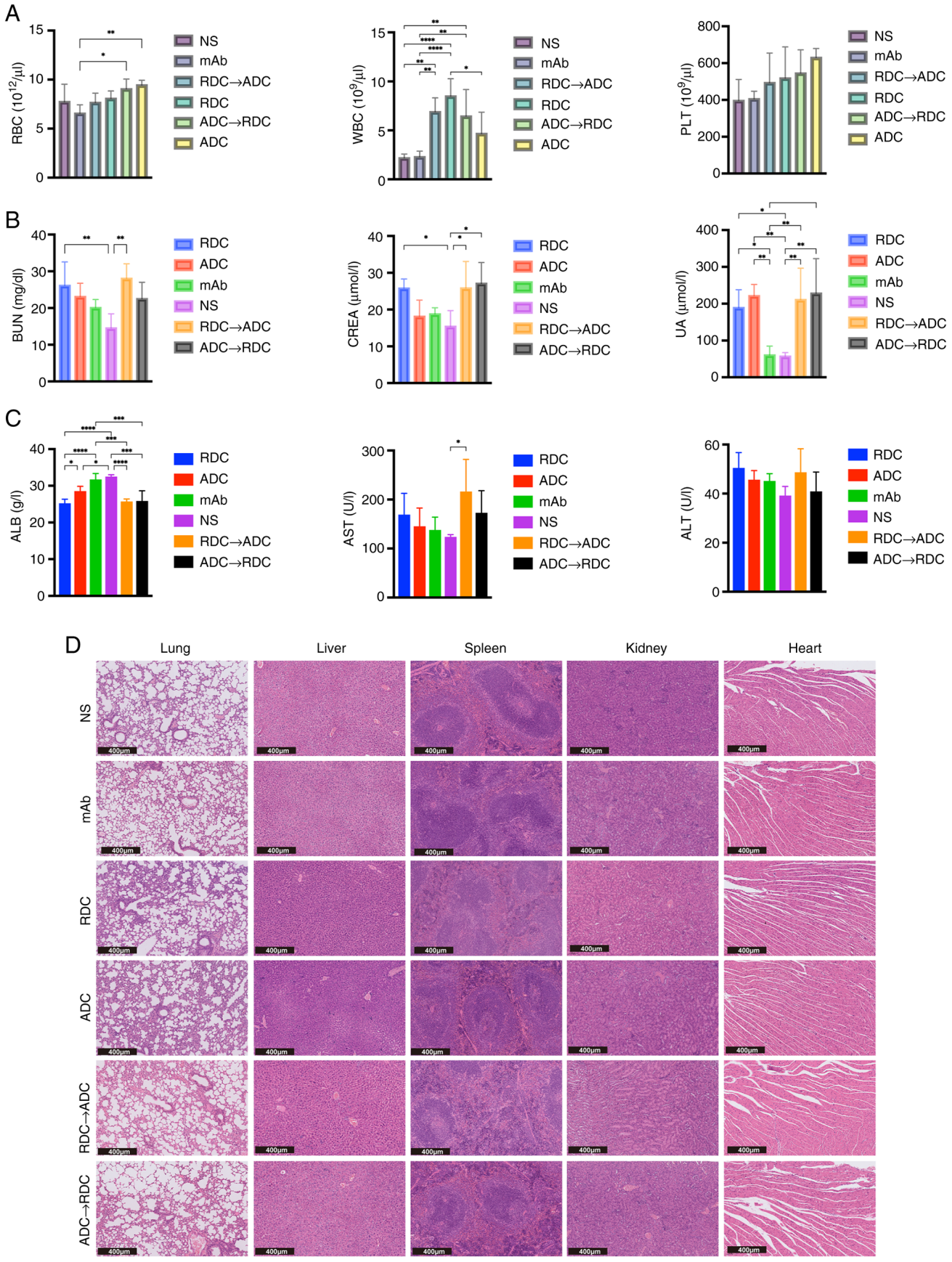

Figure 4. (A) WBC, RBC and PLT counts of each treatment group at the end of treatment (n=5 mice/group). (B) BUN, CREA and UA levels in each treatment group at the end of treatment. (C) ALB, AST and ALT levels in each treatment group at the end of treatment. (D) Representative hematoxylin and eosin staining of tissues collected from euthanized mice from each treatment group. Statistical differences across the groups were determined by one-way analysis of variance followed by Tukey's post hoc test for multiple comparisons. *P<0.05, **P<0.01, ***P<0.001, ****P<0.0001. ADC, antibody-drug conjugate; ALB, albumin; ALT alanine amino transferase; AST, aspartate aminotransferase; BUN, blood urea nitrogen; CREA, creatinine; mAb, monoclonal antibody; NS, normal saline; PLT, platelet; RBC, red blood cell; RDC, radionuclide-drug conjugate; UA, uric acid; WBC, white blood cell.

Discussion

To the best of our knowledge, the present study is the first preclinical experiment comparing the efficacy and safety of ADCs, RDCs and their sequential combinations targeting the same receptor. The current study systematically evaluated the therapeutic efficacy of CLDN18.2-targeted ADC, RDC and various sequential combination therapies in a preclinical GC mouse model. The results showed that the ADC group was significantly associated with improved key efficacy endpoints, such as OS and CR rates, compared with those in both the RDC and RDC→ADC groups, alongside a more favorable safety profile. Although the survival benefit of the ADC→RDC combination treatment did not significantly differ from that of ADC monotherapy, the combination therapy group exhibited higher blood toxicity, and liver and kidney damage. These findings suggest that ADC monotherapy may have superior efficacy and safety in the current preclinical model. From a mechanistic perspective, the therapeutic advantage of ADCs primarily arises from their ability to precisely deliver cytotoxic drugs via antibody-targeted delivery (53). Additionally, the cleavable linker of ADCs can generate a 'bystander effect', which helps eliminate nearby antigen-negative cells (54). In the present study, a 60% CR rate was maintained for 5 months following ADC monotherapy, which is closely associated with high stability of the CLDN18.2 antigen during the treatment period. However, existing clinical studies have indicated that prolonged use of ADCs may lead to acquired resistance through mechanisms such as abnormal antigen internalization or lysosomal escape (55,56). The absence of such acquired resistance in the current study may be linked to the relatively low dosing frequency (only two administrations) and short observation period in the current study. Future studies should assess the long-term effects of treatment on drug resistance.

In the combination therapy strategy, the tumor CR rate in the ADC→RDC group was higher than that in the RDC→ADC group, with a 40% difference. Although the sample size (n=5/group) in the current study was limited, resulting in a low statistical power, and this difference did not reach statistical significance after correction for multiple comparisons, the magnitude of the observed trend and effect size still suggests that the sequence of administration may be a potential factor influencing antitumor efficacy. This finding provides a valuable preliminary hypothesis for future large-scale studies. Furthermore, based on previous literature, it may be hypothesized that administering ADC first could create a favorable condition for subsequent RDC therapy through several potential mechanisms: i) Rapidly reducing tumor burden by downregulating hypoxia-inducible factor 1α expression, which alleviates the tumor hypoxic microenvironment (57), thereby enhancing the sensitivity of the tumor to radiotherapy (58); ii) ADC-induced G_2/M phase cell cycle arrest, which makes tumor cells more sensitive during radiotherapy (59); and iii) conversely, if RDC therapy is used first, it may induce radiation-induced fibrosis, which increases the hydraulic pressure of the tumor stroma, hindering the intratumoral penetration of ADC drugs (60). These potential mechanisms may explain the efficacy trend observed in the current study.

Previous studies have shown that ADC and RDC monotherapies demonstrate relatively good efficacy in CLDN18.2-targeted therapy (61,62). For example, [^{177}Lu]Lu-TST001 has exhibited marked efficacy and low short-term toxicity in preclinical GC models (41), although no long-term toxicity has been observed. In the current study, a 5-month long-term observation revealed that although RDC treatment effectively inhibited tumor growth, it was associated with relatively high hematological and visceral toxicity. This suggests that CLDN18.2-RDC therapy requires further optimization to reduce side effects. Moreover, in a previous study, CLDN18.2-307-ADC induced sustained tumor regression in cell-derived xenograft and patient-derived xenograft models with manageable toxicity (40). These findings are consistent with the results of this study, where a 60% CR rate was observed in the ADC treatment group, and the tumors remained stable after regression without recurrence. However, the prolonged use of ADC may result in resistance issues, including target antigen downregulation, antigen loss or mutations, leading to a gradual reduction in therapeutic efficacy (63). Therefore, the potential efficacy of the ADC→RDC combination therapy in resistant patients is of particular importance. By initially using ADC to reduce tumor burden and improve the microenvironment, subsequent RDC treatment may eliminate residual tumor cells more effectively, thereby lowering recurrence risk (64). This treatment strategy is especially suitable for ADC-resistant patients for whom RDC may serve as an effective adjunct therapy.

The National Medical Products Administration has approved CLDN18.2 mAb (zolbetuximab) in combination with fluoropyrimidine and platinum-based chemotherapy as a first-line treatment for locally advanced unresectable or metastatic CLDN18.2-positive, human epidermal growth factor receptor 2 (HER2)-negative gastric or gastroesophageal junction adenocarcinoma. However, in the present study, the mAb-CLDN18.2 monotherapy group did not show any significant antitumor efficacy. This outcome may be attributed to the relatively low doses administered. The conventional clinical dose is 800 mg/m^2 (65,66), whereas the dose used in the current study was only 50 nmol/kg. At such a low dose, the antibody may not achieve sufficient target engagement or elicit a robust immune response to produce antitumor effects as monotherapy. Future studies should consider using higher doses in order to observe more pronounced therapeutic outcomes.

The present study has several design limitations that warrant further discussion. First, owing to experimental constraints, the pharmacokinetic characteristics and maximum tolerated doses of different treatment regimens were not systematically compared, which may affect the generalizability of the conclusions regarding efficacy and safety. To control for core variables, a uniform dose of 150 μg (50 nmol/kg) mAb was used as a baseline. This decision was based on the following considerations: First, the fixed DAR (DAR=2) of ADCs is structurally consistent with the radionuclide-to-antibody labeling ratio (value=2) of RDCs. Second, prior studies have shown that 1.1 MBq ^{177}Lu-labeled full antibodies (150 μg) effectively suppress tumor growth with good tolerability (51,52). Although there are differences in the mechanisms of action between ADCs and RDCs (67,68), an equal antibody dosage ensures comparability in target occupancy, thereby providing a basis for a fair evaluation of the antitumor activity of different carrier systems. Although the absence of pharmacokinetic parameters limits the depth of mechanistic interpretation, the cross-modal

drug comparison paradigm and sequential strategy established in the present study remain valuable and may provide insights for future studies.

Second, the present study used only a single conventional tumor model and did not account for the potential effect of different GC subtypes or resistance models on treatment outcomes. Tumor heterogeneity suggests that a single model may not fully capture the diversity in clinical treatments. Therefore, future studies should incorporate multi-model validation, particularly the use of resistance models, to enhance the generalizability of the findings. Nevertheless, although the results obtained from a single model may not be broadly applicable, the favorable outcomes observed with both ADC and ADC→RDC sequential combination therapies in the current study offer valuable insights and guidance for subsequent validation in resistance models and the development of treatment strategies for advanced clinical patients.

Third, all efficacy and toxicity observations were derived from the NUGC-4-CLDN18.2 xenograft model, which differs fundamentally from human GC in several key aspects: i) Tumor microenvironment: The murine model lacks the complex human tumor microenvironment that regulates drug response and toxicity profiles in patients. ii) Pharmacokinetic and pharmacodynamic disparities: Interspecies differences in drug metabolism, distribution and elimination may notably alter treatment outcomes. iii) CLDN18.2 expression heterogeneity: Human GC demonstrates variable CLDN18.2 expression patterns (such as focal vs. diffuse and high vs. low) and potentially treatment-modifying co-mutations (including in HER2 and TP53), whereas the NUGC-4-CLDN18.2 model represents only a single CLDN18.2-overexpressing cell line, thereby limiting the generalizability of the findings across different patient subgroups.

Fourth, the study included multiple groups, but the sample size was limited (n=5/group), which resulted in a low statistical power. After correction for multiple comparisons, some intergroup differences in the survival analysis did not reach statistical significance, and thus, these specific findings were only presented as trends. Future studies will require a larger sample size to validate these findings.

Finally, the current study did not explore the potential acquired resistance mechanisms to ADC therapy, which is directly relevant to the development of subsequent treatment strategies for patients with resistance in clinical settings. These limitations underscore the need for cautious interpretation of the results and emphasize the requirement for future clinical studies to establish the comparative efficacy and safety of ADC and RDC strategies in patients with CLDN18.2-positive GC.

In conclusion, the present preclinical findings suggest that ADC monotherapy may demonstrate superior efficacy and safety profiles when compared with RDC monotherapy. Sequential combination therapy starting with ADC appears to be more favorable than that which starts with RDC. Although ADC→RDC sequential therapy did not significantly outperform ADC monotherapy in this model, it may serve as an effective subsequent treatment strategy.

Acknowledgements

Not applicable.

Funding

The present study was financially supported by the Key Laboratory of Nuclear Technology (grant nos. 2021HYX001 and 2022 HYX015), the Mianyang Science and Technology Bureau (Minyang Science and Technology Program; grant no. 2023ZYDF073) and the Mianyang Municipal Finance Bureau (grant no. miancaijian2022-186).

Availability of data and materials

The data generated in the present study may be requested from the corresponding author.

Authors' contributions

XD, XY and YY conceived and designed the study. HD, XH, BL, LR, JW, MT, DW, YZhu, JL and XY performed the experiments. HD, XH, BL YZha, TD, and XY analyzed the data. HD was a major contributor in writing the manuscript. XD and XY assume overall responsibility for the manuscript. XD and HD confirm the authenticity of all the raw data. XD, HD, YZha and TD were responsible for supervision and funding acquisition. All authors read and approved the final manuscript.

Ethics approval and consent to participate

The present study was approved by the Ethical Review Board of Mianyang Central Hospital (approval no. S20240210).

Patient consent for publication

Not applicable.

Competing interests

The authors declare that they have no competing interests.

References

1. Bray F, Laversanne M, Sung H, Ferlay J, Siegel RL, Soerjomataram I and Jemal AL: Global cancer statistics 2022: GLOBOCAN estimates of incidence and mortality worldwide for 36 cancers in 185 countries. CA Cancer J Clin 74: 229-263, 2024.
2. Sexton RE, Al Hallak MN, Diab M and Azmi AS: Gastric cancer: A comprehensive review of current and future treatment strategies. Cancer Metastasis Rev 39: 1179-1203, 2020.
3. Smyth EC, Nilsson M, Grabsch HI, van Grieken NC and Lordick F: Gastric cancer. Lancet 396: 635-648, 2020.
4. Ling Q, Huang ST, Yu TH, Liu HL, Zhao LY, Chen XL, Liu K, Chen XZ, Yang K, Hu JK, *et al*: Optimal timing of surgery for gastric cancer after neoadjuvant chemotherapy: A systematic review and meta-analysis. World J Surg Oncol 21: 377, 2023.
5. Merchant SJ, Kong W, Mahmud A, Booth CM and Hanna TP: Palliative radiotherapy for esophageal and gastric cancer: Population-based patterns of utilization and outcomes in Ontario, Canada. J Palliat Care 38: 157-166, 2023.
6. Haggstrom L, Chan WY, Nagrial A, Chantrill LA, Sim HW, Yip D and Chin V: Chemotherapy and radiotherapy for advanced pancreatic cancer. Cochrane Database Syst Rev 12: CD011044, 2024.
7. Yan SY and Fan JG: Application of immune checkpoint inhibitors and microsatellite instability in gastric cancer. World J Gastroenterol 30: 2734-2739, 2024.

8. Nie Y, Schalper KA and Chiang A: Mechanisms of immunotherapy resistance in small cell lung cancer. Cancer Drug Resist 7: 55, 2024.
9. Xu W, Li B, Xu M, Yang T and Hao X: Traditional Chinese medicine for precancerous lesions of gastric cancer: A review. Biomed Pharmacother 146: 112542, 2022.
10. Liu Y, Huang T, Wang L, Wang Y, Liu Y, Bai J, Wen X, Li Y, Long K and Zhang H: Traditional Chinese Medicine in the treatment of chronic atrophic gastritis, precancerous lesions and gastric cancer. J Ethnopharmacol 337: 118812, 2025.
11. Dai Z, Tan C, Wang J, Wang Q, Wang Y, He Y, Peng Y, Gao M, Zhang Y, Liu L, *et al*: Traditional Chinese medicine for gastric cancer: An evidence mapping. Phytother Res 38: 2707-2723, 2024.
12. Gao S, Xu T, Wang W, Li J, Shan Y, Wang Y and Tan H: Polysaccharides from Anemarrhena asphodeloides Bge, the extraction, purification, structure characterization, biological activities and application of a traditional herbal medicine. Int J Biol Macromol 311: 143497, 2025.
13. Gao S, Wang Y, Shan Y, Wang W, Li J and Tan H: Rhizoma Coptidis polysaccharides: Extraction, separation, purification, structural characteristics and bioactivities. Int J Biol Macromol 320: 145677, 2025.
14. Wang G, Huang Y, Zhou L, Yang H, Lin H, Zhou S, Tan Z and Qian J: Immunotherapy and targeted therapy as first-line treatment for advanced gastric cancer. Crit Rev Oncol Hematol 198: 104197, 2024.
15. Zhang X, Yang L, Liu S, Cao LL, Wang N, Li HC and Ji JF: Interpretation on the report of global cancer statistics 2022. Zhonghua Zhong Liu Za Zhi 46: 710-721, 2024 (In Chinese).
16. Inamoto R, Takahashi N and Yamada Y: Claudin18.2 in advanced gastric cancer. Cancers (Basel) 15: 5742, 2023.
17. Sahin U, Koslowski M, Dhaene K, Usener D, Brandenburg G, Seitz G, Huber C and Türeci O: Claudin-18 splice variant 2 is a pan-cancer target suitable for therapeutic antibody development. Clin Cancer Res 14: 7624-7634, 2008.
18. Baek JH, Park DJ, Kim GY, Cheon J, Kang BW, Cha HJ and Kim JG: Clinical implications of claudin18.2 expression in patients with gastric cancer. Anticancer Res 39: 6973-6979, 2019.
19. Bunga OD and Danilova NV: Claudin-18.2 and gastric cancer: From physiology to carcinogenesis. Arkh Patol 86: 92-99, 2024 (In Russian).
20. Mathias-Machado MC, de Jesus VHF, Jácome A, Donadio MD, Aruquipa MPS, Fogacci J, Cunha RG, da Silva LM and Peixoto RD: Claudin 18.2 as a new biomarker in gastric cancer-what should we know? Cancers (Basel) 16: 679, 2024.
21. Nakayama I, Qi C, Chen Y, Nakamura Y, Shen L and Shitara K: Claudin 18.2 as a novel therapeutic target. Nat Rev Clin Oncol 21: 354-369, 2024.
22. Tojjari A, Idrissi YA and Saeed A: Emerging targets in gastric and pancreatic cancer: Focus on claudin 18.2. Cancer Lett 611: 217362, 2024.
23. Seckin Y, Arici S, Harputluoglu M, Yonem O, Yilmaz A, Ozer H, Karincaoglu M and Demirel U: Expression of claudin-4 and beta-catenin in gastric premalignant lesions. Acta Gastroenterol Belg 72: 407-412, 2009.
24. Konno H, Lin T, Wu R, Dai X, Li S, Wang G, Chen M, Li W, Wang L, Sun BC, *et al*: ZL-1211 exhibits robust antitumor activity by enhancing ADCC and activating NK Cell-mediated inflammation in CLDN18.2-High and -Low expressing gastric cancer models. Cancer Res Commun 2: 937-950, 2022.
25. Kubota Y, Kawazoe A, Mishima S, Nakamura Y, Kotani D, Kuboki Y, Bando H, Kojima T, Doi T, Yoshino T, *et al*: Comprehensive clinical and molecular characterization of claudin 18.2 expression in advanced gastric or gastroesophageal junction cancer. ESMO Open 8: 100762, 2023.
26. Castillo DR, Guo M, John Kim K II, Zhong H, Brar G, Wu S, Mannan R, Cecilia Lau S, Xing Y and Peter Wu S: Association of Claudin18.2 expression, PD-L1, and prognostic implications in gastric and gastroesophageal junction cancers. J Clin Oncol 43: e16094, 2025.
27. Wang C, Wang Y, Chen J, Wang Y, Pang C, Liang C, Yuan L and Ma Y: CLDN18.2 expression and its impact on prognosis and the immune microenvironment in gastric cancer. BMC Gastroenterol 23: 283, 2023.
28. Rha SY, Kwon WS, Lee CK, Jung M, Shin S, Kim H, Park S, Yoo JH and Kim H: Co-expressing pattern of multiple biomakers and dynamic change of Claudin18.2 expression after systemic chemotherapy in advanced gastric cancer. J Clin Oncol 43: 4037, 2025.
29. Lordick F, Van Cutsem E, Shitara K, Xu RH, Ajani JA, Shah MA, Oh M, Ganguli A, Chang L, Rhoten S, *et al*: Health-related quality of life in patients with CLDN18.2-positive, locally advanced unresectable or metastatic gastric or gastroesophageal junction adenocarcinoma: Results from the SPOTLIGHT and GLOW clinical trials. ESMO Open 9: 103663, 2024.
30. Kim HD, Choi E, Shin J, Lee IS, Ko CS, Ryu MH and Park YS: Clinicopathologic features and prognostic value of claudin 18.2 overexpression in patients with resectable gastric cancer. Sci Rep 13: 20047, 2023.
31. Pellino A, Brignola S, Riello E, Niero M, Murgioni S, Guido M, Nappo F, Businello G, Sbaraglia M, Bergamo F, *et al*: Association of CLDN18 protein expression with clinicopathological features and prognosis in advanced gastric and gastroesophageal junction adenocarcinomas. J Pers Med 11: 1095, 2021.
32. Waters R, Sewastjanow-Silva M, Yamashita K, Abdelhakeem A, Iwata KK, Moran D, Elsouda D, Guerrero A, Pizzi M, Vicentini ER, *et al*: Retrospective study of claudin 18 isoform 2 prevalence and prognostic association in gastric and gastroesophageal junction adenocarcinoma. JCO Precis Oncol 8: e2300543, 2024.
33. Ungureanu BS, Lungulescu CV, Pirici D, Turcu-Stiolica A, Gheonea DI, Sacerdotianu VM, Liliac IM, Moraru E, Bende F and Saftoiu A: Clinicopathologic relevance of claudin 18.2 expression in gastric cancer: A Meta-analysis. Front Oncol 11: 643872, 2021.
34. Gao J, Wang Z, Jiang W, Zhang Y, Meng Z, Niu Y, Sheng Z, Chen C, Liu X, Chen X, *et al*: CLDN18.2 and 4-1BB bispecific antibody givastomig exerts antitumor activity through CLDN18.2-expressing tumor-directed T-cell activation. J Immunother Cancer 11: e006704, 2023.
35. Optimism Surrounds Claudin 18.2 ADC. Cancer Discov 14: 12, 2024.
36. Li D, Ding L, Chen Y, Wang Z, Zeng Z, Ma X, Huang H, Li H, Qian X, Yang Z and Zhu H: Exploration of radionuclide labeling of a novel scFv-Fc fusion protein targeting CLDN18.2 for tumor diagnosis and treatment. Eur J Med Chem 266: 116134, 2024.
37. Sahin U, Türeci Ö, Manikhas G, Lordick F, Rusyn A, Vynnychenko I, Dudov A, Bazin I, Bondarenko I, Melichar B, *et al*: FAST: A randomised phase II study of zolbetuximab (IMAB362) plus EOX versus EOX alone for first-line treatment of advanced CLDN18.2-positive gastric and gastro-oesophageal adenocarcinoma. Ann Oncol 32: 609-619, 2021.
38. Shitara K, Kawazoe A, Hirakawa A, Nakanishi Y, Furuki S, Fukuda M, Ueno Y, Raizer J and Arozullah A: Phase 1 trial of zolbetuximab in Japanese patients with CLDN18.2+ gastric or gastroesophageal junction adenocarcinoma. Cancer Sci 114: 1606-1615, 2023.
39. Klempner SJ, Lee KW, Shitara K, Metges JP, Lonardi S, Ilson DH, Fazio N, Kim TY, Bai LY, Moran D, *et al*: ILUSTRO: Phase II multicohort trial of zolbetuximab in patients with advanced or metastatic claudin 18.2-Positive gastric or gastroesophageal junction adenocarcinoma. Clin Cancer Res 29: 3882-3891, 2023.
40. O'Brien NA, McDermott MSJ, Zhang J, Gong KW, Lu M, Hoffstrom B, Luo T, Ayala R, Chau K, Liang M, *et al*: Development of a novel CLDN18.2-directed monoclonal antibody and antibody-drug conjugate for treatment of CLDN18.2-positive cancers. Mol Cancer Ther 22: 1365-1375, 2023.
41. Zeng Z, Li L, Tao J, Liu J, Li H, Qian X, Yang Z and Zhu H: [^{177}Lu]Lu-labeled anti-claudin-18.2 antibody demonstrated radioimmunotherapy potential in gastric cancer mouse xenograft models. Eur J Nucl Med Mol Imaging 51: 1221-1232, 2024.
42. Dumontet C, Reichert JM, Senter PD, Lambert JM and Beck A: Antibody-drug conjugates come of age in oncology. Nat Rev Drug Discov 22: 641-661, 2023.
43. Lu X, Zhu Y, Deng X, Kong F, Xi C, Luo Q and Zhu X: Development of a supermolecular Radionuclide-drug conjugate system for integrated radiotheranostics for Non-small cell lung cancer. J Med Chem 67: 11152-11167, 2024.
44. Chau CH, Steeg PS and Figg WD: Antibody-drug conjugates for cancer. Lancet 394: 793-804, 2019.
45. Zhou L, Lu Y, Liu W, Wang S, Wang L, Zheng P, Zi G, Liu H, Liu W and Wei S: Drug conjugates for the treatment of lung cancer: From drug discovery to clinical practice. Exp Hematol Oncol 13: 26, 2024.
46. Khongorzul P, Ling CJ, Khan FU, Ihsan AU and Zhang J: Antibody-drug conjugates: A comprehensive review. Mol Cancer Res 18: 3-19, 2020.
47. Zhou KI, Strickler JH and Chen H: Targeting Claudin-18.2 for cancer therapy: Updates from 2024 ASCO annual meeting. J Hematol Oncol 17: 73, 2024.

48. Yeh CL, Pai MH, Li CC, Tsai YL and Yeh SL: Effect of arginine on angiogenesis induced by human colon cancer: In vitro and in vivo studies. J Nutr Biochem 21: 538-543, 2010.
49. Kinjo K, Kizaki M, Muto A, Fukuchi Y, Umezawa A, Yamato K, Nishihara T, Hata J, Ito M, Ueyama Y, *et al*: Arsenic trioxide (As2O3)-induced apoptosis and differentiation in retinoic acid-resistant acute promyelocytic leukemia model in hGM-CSF-producing transgenic SCID mice. Leukemia 14: 431-438, 2000.
50. Yao Y, Ren Y, Hou X, Zhu J, Ma X, Liu S, Liu T, Zhang Q, Ma X, Yang Z, *et al*: Construction and preclinical evaluation of a zirconium-89 labelled monoclonal antibody targeting PD-L2 in lung cancer. Biomed Pharmacother 168: 115602, 2023.
51. Du H, Hao X, Lin B, Tang M, Wang D, Yang X, Wang J, Qin L, Yang Y and Du X: 177Lu-labeled anticlaudin 6 monoclonal antibody for targeted therapy in esophageal cancer. J Nucl Med 66: 377-384, 2025.
52. Zheng L, Li C, Yang X, Liu J, Wang G, Zhou Z, Zhu X, Gong J and Yang J: GD2-targeted theranostics of neuroblastoma with [^{64}Cu]Cu/[^{177}Lu]Lu-hu3F8. Eur J Nucl Med Mol Imaging 52: 1764-1777, 2025.
53. Drago JZ, Modi S and Chandarlapaty S: Unlocking the potential of antibody-drug conjugates for cancer therapy. Nat Rev Clin Oncol 18: 327-344, 2021.
54. Baah S, Laws M and Rahman KM: Antibody-Drug Conjugates-A tutorial review. Molecules 26: 2943, 2021.
55. Chen YF, Xu YY, Shao ZM and Yu KD: Resistance to antibody-drug conjugates in breast cancer: mechanisms and solutions. Cancer Commun (Lond) 43: 297-337, 2023.
56. Díaz-Rodríguez E, Gandullo-Sánchez L, Ocaña A and Pandiella A: Novel ADCs and strategies to overcome resistance to Anti-HER2 ADCs. Cancers (Basel) 14: 154, 2021.
57. Jain RK: Normalizing tumor microenvironment to treat cancer: bench to bedside to biomarkers. J Clin Oncol 31: 2205-2218, 2013.
58. Beckers C, Pruschy M and Vetrugno I: Tumor hypoxia and radiotherapy: A major driver of resistance even for novel radiotherapy modalities. Semin Cancer Biol 98: 19-30, 2024.
59. Pawlik TM and Keyomarsi K: Role of cell cycle in mediating sensitivity to radiotherapy. Int J Radiat Oncol Biol Phys 59: 928-942, 2004.
60. Straub JM, New J, Hamilton CD, Lominska C, Shnayder Y and Thomas SM: Radiation-induced fibrosis: Mechanisms and implications for therapy. J Cancer Res Clin Oncol 141: 1985-1994, 2015.
61. Yamamoto K, Nakayama I and Shitara K: A new molecular targeted agent for gastric Cancer-The Anti-Claudin 18.2 antibody, zolbetuximab. Gan To Kagaku Ryoho 51: 1111-1118, 2024 (In Japanese).
62. Liu Y, Wang X, Zhang N, He S, Zhang J, Xu X and Song S: Utility of 131I-HLX58-Der for the precision treatment: Evaluation of a preclinical radio-antibody-drug-conjugate approach in mouse models. Int J Nanomedicine 20: 723-739, 2025.
63. Chang HL, Schwettmann B, McArthur HL and Chan IS: Antibody-drug conjugates in breast cancer: Overcoming resistance and boosting immune response. J Clin Invest 133: e172156, 2023.
64. Jiao J, Qian Y, Lv Y, Wei W, Long Y, Guo X, Buerliesi A, Ye J, Han H, Li J, *et al*: Overcoming limitations and advancing the therapeutic potential of antibody-oligonucleotide conjugates (AOCs): Current status and future perspectives. Pharmacol Res 209: 107469, 2024.
65. Shah MA, Shitara K, Ajani JA, Bang YJ, Enzinger P, Ilson D, Lordick F, Van Cutsem E, Gallego Plazas J, Huang J, *et al*: Zolbetuximab plus CAPOX in CLDN18.2-positive gastric or gastroesophageal junction adenocarcinoma: The randomized, phase 3 GLOW trial. Nat Med 29: 2133-2141, 2023.
66. Shitara K, Shah MA, Lordick F, Van Cutsem E, Ilson DH, Klempner SJ, Kang YK, Lonardi S, Hung YP, Yamaguchi K, *et al*: Zolbetuximab in gastric or gastroesophageal junction adenocarcinoma. N Engl J Med 391: 1159-1162, 2024.
67. Hammood M, Craig AW and Leyton JV: Impact of endocytosis mechanisms for the receptors targeted by the currently approved Antibody-drug conjugates (ADCs)-A necessity for future ADC research and development. Pharmaceuticals (Basel) 14: 674, 2021.
68. Zhang S, Wang X, Gao X, Chen X, Li L, Li G, Liu C, Miao Y, Wang R and Hu K: Radiopharmaceuticals and their applications in medicine. Signal Transduct Target Ther 10: 1, 2025.